Journal of Power Sources 269 (2014) 317–333

Contents lists available at ScienceDirect

Journal of Power Sources

journal homepage: www.elsevier.com/locate/jpowsour

Open circuit voltage characterization of lithium-ion batteries

B. Pattipati, B. Balasingam*, G.V. Avvari, K.R. Pattipati, Y. Bar-Shalom

Department of Electrical and Computer Engineering, University of Connecticut, 371 Fairfield Way, U-2157, Storrs, CT 06269, USA

HIGHLIGHTS

- A novel *normalized OCV modeling* approach is developed.
- The normalized OCV modeling is stable over temperature changes and battery aging.
- The importance of battery capacity in OCV modeling is demonstrated.
- The hysteresis is marginalized by having symmetric charging and discharging data.
- Proposed OCV modeling is validated for different chemistries, temperatures and aging.

ARTICLE INFO

Article history:
Received 19 April 2014
Received in revised form
26 June 2014
Accepted 27 June 2014
Available online 9 July 2014

Keywords:
Li-ion battery
Open circuit voltage (OCV)
State of charge (SOC)
Battery management system (BMS)
Battery fuel gauge (BFG)

ABSTRACT

Several aspects of the open circuit voltage (OCV) characterization of Li-ion batteries as it applies to battery fuel gauging (BFG) in portable applications are considered in this paper. Accurate knowledge of the nonlinear relationship between the OCV and the state of charge (SOC) is required for adaptive SOC tracking during battery usage. BFG in portable applications requires this OCV–SOC characterization to meet additional constraints: (i) The OCV–SOC characterization has to be defined with a minimum number of parameters; (ii) It should be easily computable and invertible with few operations; and (iii) Computation of the model, its derivative and its inverse should be possible in a numerically stable way. With the help of OCV–SOC characterization data collected from 34 battery cells each at 16 different temperatures ranging from −25 °C to 50 °C, we present the following results in this paper: (a) A robust normalized OCV modeling approach that dramatically reduces the number of OCV–SOC parameters and as a result simplifies and generalizes the BFG across temperatures and aging, (b) Several novel functions for OCV modeling, (c) Efficient methods to simplify the computations of OCV functions, (d) Novel methods for OCV parameter estimation, and (e) A detailed performance analysis.

1. Introduction

Rechargeable Lithium-ion batteries are widely used in electric vehicles, personal/wearable electronic devices, household appliances, aerospace equipment, grid storage, and so on. Estimating the state of charge (SOC) and state of health (SOH), known as battery fuel gauging [1–3], is an important function in equipment powered by rechargeable batteries. The OCV is a measure of the electromotive force (EMF) of the battery, which is known to have a monotonic relationship with the SOC of the battery, hence, estimating SOC must have been a straightforward, voltage-look-up process. However, due to the variable internal resistance, capacity, hysteresis and relaxation effects of the battery, the BFG involves many components as outlined in Fig. 1; please see Ref. [2] for a detailed description of the function of each block. The focus of the paper is on estimating the parameters of the OCV–SOC characterization.

Existing OCV modeling approaches can be broadly classified into chemistry-based and Current–Voltage based approaches. In chemistry-based approaches [4], the OCV of each electrode (anode and cathode w.r.t. some reference) is expressed as a function of the utilization of the electrode (the lithium concentration in the electrode normalized by the maximum possible concentration) or the SOC of each electrode. It is generally assumed that this anode and cathode SOC varies linearly with the cell SOC [5]. Subsequently, the difference between the OCV of the anode and cathode gives the OCV of the complete cell. High current rates (i.e., near the rated maximum) have been shown to affect the macroscopic processes in

* Corresponding author.
E-mail addresses: bharath@engr.uconn.edu (B. Pattipati), bala@engr.uconn.edu, bhalakumar@gmail.com (B. Balasingam), vinod@engr.uconn.edu (G.V. Avvari), krishna@engr.uconn.edu (K.R. Pattipati), ybs@engr.uconn.edu (Y. Bar-Shalom).

http://dx.doi.org/10.1016/j.jpowsour.2014.06.152
0378-7753/

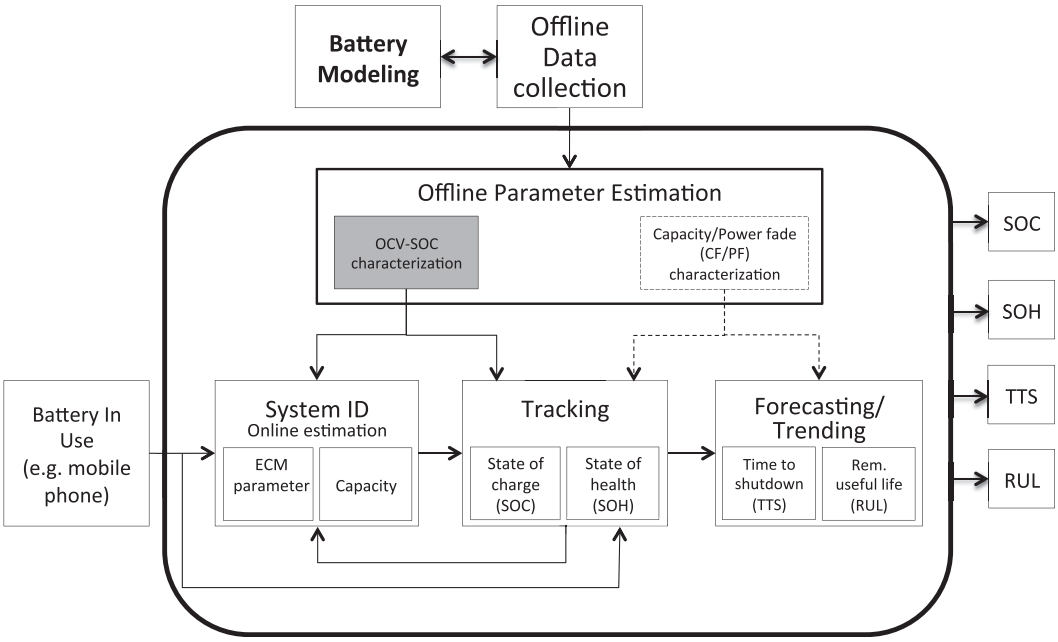

Fig. 1. Elements of a BFG. The focus of this paper, OCV–SOC characterization is shaded in gray. Details of System ID block can be found in Refs. [1,2] and the details of SOC tracking block can be found in Ref. [3].

a way that the OCV hysteresis vanishes for Li-ion cells, which regularly show OCV hysteresis after low current application [6]. Roscher et al. [7] conducted OCV (full and partial charge–discharge cycle) tests on Lithium ion phosphate ($LiFePO_4$) batteries to characterize the hysteresis and recovery effects. The final OCV model is constructed by concatenating the actual SOC, the recovery factor and the hysteresis factor. Our focus in this paper is on Current–Voltage based OCV–SOC characterization.

The Current–Voltage based OCV–SOC characterization can be summed by two simple steps:

(i) Collect pairs of {OCV, SOC} values, spanning the entire range of $SOC \triangleq [0, 1]$
(ii) Use the above data to estimate the parameters of the function $OCV = f(SOC)$ for a hypothesized function f.

There are challenges in both of the above steps. The objective of this paper is to detail them and discuss ways to address them.

Fig. 2 shows the equivalent circuits of a battery when it is experiencing dynamic current versus when it is rested [1]. When the battery is experiencing dynamic current, the voltage difference between OCV, $V_\circ(s[k])$, where, $s[k]$ is the SOC at the discrete time k, and the measured terminal voltage $v[k]$ becomes higher. When the current $i[k]$ becomes zero, the battery starts to "relax", i.e., the capacitors $C_1,\ldots,C_N$ start to discharge through R_1, …, R_N, respectively. The battery is said to be in a "rest state" when $i[k] = 0$ for longer than the multiple (typically ≥ 5) of the largest time constant R_iC_i in the equivalent circuit model, i.e., until all the capacitors $C_1,\ldots,C_N$ are fully discharged. However, the OCV is still unreachable at the terminal even after the battery is rested, due to the hysteresis voltage $h[k]$.

The hysteresis, also known as "voltage pull" – a derivative expression, depends on the direction, magnitude and duration of the preceding current as well as on the SOC. Hysteresis is known to result from thermodynamical entropic effects, mechanical stress, and microscopic distortions within the active electrode materials, which perform a two-phase transition during lithium insertion/extraction [6]. Thus, knowing the exact value of hysteresis is impractical. However, since the direction of the hysteresis voltage is opposite during charging and discharging,[1] the OCV (at a certain SOC) can be approximately estimated by averaging the measured terminal voltage during charging and discharging when the entire experiment is performed using the same magnitude of current. Usually, a smaller current[2] is required in order to reach the OCV at both ends, i.e., to measure OCV from $V_\circ(0)$ to $V_\circ(1)$.

The SOC of the battery for OCV–SOC characterization is computed through Coulomb counting, which keeps track of the amount of Coulombs extracted from/inserted into the battery and computes the SOC as a ratio of remaining Coulombs and battery capacity. Hence, the knowledge of battery capacity is crucial for accurate OCV–SOC characterization. Usually, the OCV–SOC characterization is performed on a new battery, hence, manufacturer specified capacity (also known as "rated capacity") or Coulomb counting from a fully charged battery to a fully empty battery at very low current values will serve as a fairly accurate estimate of the initial battery capacity.

However, the battery capacity is known to fade over time; hence, the BFG[3] needs to account for the capacity fade over time. At this point, the OCV–SOC characterization made using incorrect capacity will become more and more unsuitable. We will elaborate on this point later in this paper.

The conclusion from the existing literature is that the OCV–SOC characterization changes with battery temperature. Hence, many existing approaches suggested computing OCV parameters at

[1] It must be noted that the hysteresis voltage reversal is delayed, i.e., when the current reversal occurs, the hysteresis reversal follows with a delay.
[2] Using high current in OCV experiments will prevent reaching full battery (SOC = 1) or empty battery (SOC = 0).
[3] A BFG needs the battery capacity information in the "Coulomb counting equation" or process model, see Ref. [3].

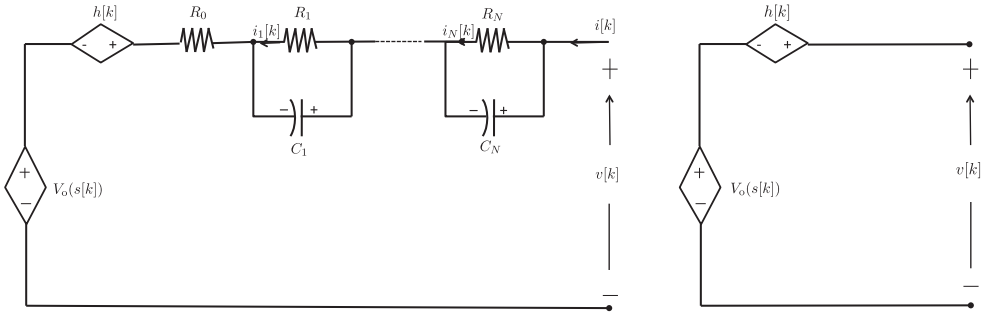

(a) Battery under dynamic current (b) Rested battery

Fig. 2. Equivalent circuit of a battery when it is experiencing dynamic current vs. when it is rested. The measurable voltage across battery terminals is indicated by $v[k]$ and the current through the battery is $i[k]$. The currents through R_1, …, R_N are indicated by $i_1[k]$, …, $i_N[k]$, $h[k]$ denotes hysteresis and R_0 denotes the series resistance.

intermediate temperatures spanning possible battery usage. The OCV parameters at any other temperature are then obtained through interpolation. In these characterizations, the SOC is computed relative to a fixed (nominal) capacity of the battery, which, based on the manufacturer specifications, holds true only at the "nominal temperature" of the battery.

Hence, one of the focal points of this research, backed by data collected from 34 battery cells each at up to 16 different temperatures spanning −25 °C to 50 °C at equal steps, is to investigate if the knowledge of battery capacity at different temperatures plays a role in OCV–SOC characterization. We computed the OCV–SOC characterization curves at each temperature and analyzed the differences. Further, rather than using the rated capacity of the battery, we computed the battery capacity through slow discharge from full to empty at each temperature. The experiments were repeated on slightly older batteries as well. Our conclusion is that the OCV–SOC characterization curve remains the same, regardless of the temperature or age[4] of the battery, as long as the correct battery capacity is used in the characterization. The implication of this conclusion is significant: There is no need to repeat OCV–SOC characterization experiments at different temperatures—doing so at one temperature is sufficient for SOC tracking at all temperatures of battery operation as long as the capacity is estimated dynamically and continuously [1–3].

Once the pairs of {OCV, SOC} values are collected, the next step is to model these data given later in (1) as a function. From a mobile computing perspective, the following constraints are relevant in selecting such a function:

- Fewest possible parameters
- Ease of computation and inversion.

Nowadays, rechargeable Li-ion batteries are used in many small electronic devices (e.g., smart watches, Google glass, etc.) and BFG is a desired capability in these devices, however, it must be able to function with limited amount of memory and computational needs. Since many of the BFG algorithms, such as the ones in Refs. [1–3], require the computation of OCV and its derivative for a certain SOC and finding the SOC given a certain OCV (inversion of (1)), the selected OCV–SOC characterization function needs to be easily computable and invertible. The functions that we eventually select involve logarithms – we employ a computationally efficient, numerically stable approach to implementing logarithms through a Padé approximation.

[4] Our analysis on aged batteries was done using a limited amount of data, hence, the conclusion about the aged batteries must be considered preliminary.

The novel contributions and results of this paper can be summarized as follows:

1. *Normalized OCV modeling*. We show that the OCV–SOC characterization is the same for any temperature; hence, doing so at one convenient temperature is adequate for BFG at all temperatures. We also show some preliminary results that, when normalized OCV modeling is employed, the OCV–SOC characterization is unaffected by aging.
2. *New OCV–SOC models*. We analyze many models for OCV–SOC characterization and propose novel models that are suitable for mobile applications, i.e., with modest memory and computational complexity.
3. *Novel approaches for OCV model parameter estimation*. We propose several approaches for OCV parameter estimation.
4. *Performance comparison of OCV–SOC modeling as it relates to BFG*. We employ several performance evaluation metrics in order to assess the suitability of models in BFG. First, the required computational complexity of each model is summarized. Then, OCV modeling accuracy is compared at a certain complexity.

Some recent works [8–10] attempt to estimate the OCV–SOC parameters online. Online estimation of the OCV parameters helps to develop a BFG that is independent of characterization and hence applicable to *any* type of battery. A challenge in online OCV–SOC characterization is that the algorithms in Refs. [8–10] rely on the end usage data for characterization; continuous data between full (SOC = 1) and nearly empty (SOC ≈ 0) state of the battery is required for complete characterization; obtaining these data will require the end user to fully charge and fully drain the battery at least once; partial OCV–SOC characterization will affect the robustness of the BFG algorithm. In our robust BFG algorithm (summarized in Fig. 1) we assume that the OCV–SOC parameters are estimated offline and the equivalent circuit model (ECM) parameters and the capacity are estimated online; we model hysteresis as a bias and estimate it online as well. The battery capacity, ECM parameters and hysteresis drift with environmental and usage patterns and age of the battery; estimating these parameters requires full life data (which is typically several hundreds of cycles) under different environmental and usage scenarios. On the other hand, the OCV–SOC parameter estimation requires just one cycle of data; further, we show in this paper that the OCV–SOC parameters are stable in the presence of temperature changes and aging of the battery. Hence, offline estimation of the OCV parameters serves our purpose of developing a robust BFG algorithm. Further, it must be noted that the OCV parameters are needed for the (online) estimation of ECM parameters, capacity and hysteresis; accurate, offline estimated OCV parameters help to ensure the robust online

estimation of these quantities. In order to generalize the BFG for multiple battery chemistries, we propose in Ref. [11] to store a carefully selected set of OCV parameters and employ probabilistic data association (PDA) in order to associate the correct OCV parameter to the battery to be gauged.

The importance of the *total capacity* of the battery in OCV–SOC parameter estimation is not fully realized in the literature. The data for OCV–SOC model parameter estimation is obtained as follows: the OCV data is collected either by slow discharge or by intermittent resting [12]; the SOC data is computed through Coulomb counting which requires the value of battery capacity. It is important to note that the correct value of battery capacity must be used in OCV–SOC modeling; the OCV–SOC curve will be different for different values of capacity used in the computation of SOC. It is observed in Refs. [13,14] that when normalized by "specific cell capacity", the OCV–SOC curve remains the same for the same battery chemistry; this observation also implies that the OCV–SOC curve remains the same for (albeit slightly) aged batteries. We have confirmed both of these observations using 34 battery cells of 11 different chemistries at eight different temperatures and two different aging conditions. The battery capacity changes with temperature; when normalized by the capacity at the temperature, the OCV–SOC curve remains the same across temperature changes as well; this is one of the major findings in this paper. We also detail how the normalization should be done by *total capacity* of the battery; unlike discharge capacity, the total capacity is the same at a certain temperature at any discharge rate.

The rest of the paper is organized as follows: A summary of existing and some newly proposed OCV–SOC models are described in Section 2. Section 3 discusses the different OCV–SOC model parameter estimation techniques. The novel normalized OCV modeling is summarized in Section 4. In Section 5, we elucidate the different metrics for the selection of an OCV–SOC model for the BFG. Section 6 evaluates the different models based on HIL data collected across different batteries and varying operating temperatures. Finally, Section 7 concludes with a summary and future research directions.

2. OCV–SOC models

The OCV of the battery has a monotonic relationship to the SOC. This relationship, usually modeled as a function, is the backbone of a BFG. In a general form, it is written as

$$V_o(s) = f(s) \tag{1}$$

where $V_\circ(s)$ denotes the OCV and $s \in [0,1]$ denotes the SOC. In this section, we summarize important OCV–SOC functions.

2.1. Linear regression-based models

A linear OCV model satisfies

$$V_o(s) = \mathbf{p}(s)^T\mathbf{k} \tag{2}$$

where $\mathbf{p}(s)^T$ is a row vector of linear/non-linear functions of s and $\mathbf{k}$ is the OCV parameter vector. It must be noted that the above expression is linear in the parameter vector $\mathbf{k}$, not necessarily in s.

We consider the following linear-in-parameter models in our analysis with the objective of finding an appropriate model that satisfies the restrictions in the number of parameters and computational complexity while providing sufficient modeling accuracy [3,15–21]:

$$\mathbf{p}_\circ(s)^T = \begin{cases} \left[1 \quad \frac{1}{s}\right] & \text{(i) Shepherd model [15, 16]} \\ [1 \quad s] & \text{(ii) Unnewehr universal model [15, 17]} \\ [1 \quad \ln(s) \quad \ln(1-s)] & \text{(iii) Nernst model [15, 18, 19]} \\ \left[1 \quad s \quad \frac{1}{s} \quad \ln(s) \quad \ln(1-s)\right] & \text{(iv) Combined model [20]} \\ \left[1 \quad s \quad \frac{1}{s} \quad \frac{1}{s^2} \quad \frac{1}{s^3} \quad \frac{1}{s^4} \quad \ln(s) \quad \ln(1-s)\right] & \text{(v) Combined + 3 model [3]} \\ \left[1 \quad s \quad \ldots \quad s^{L_1} \quad s^{-1} \quad \ldots \quad s^{-L_2}\right] & \text{(vi) Polynomial model [21]} \\ \left[1 \quad e^s \quad \ldots \quad e^{sL_1} \quad e^{-s} \quad \ldots \quad e^{-sL_2}\right] & \text{(vii) Exponential model} \\ [T_0(s) \quad T_1(s) \quad T_2(s) \ldots \quad T_{L-1}(s)] & \text{(viii) Chebyshev model} \end{cases} \tag{3}$$

$$\mathbf{k}_\circ = [K_0\ K_1\ K_2 \ldots K_M]^T \tag{4}$$

where, $M+1$ is the length of the parameter vector $\mathbf{k}$ (for example $M=1$ for the Shepherd Model and $M = L_1 + L_2$ for the polynomial model), L is the order of the Chebyshev polynomial and T_l is the lth Chebyshev polynomial.

Next we discuss some of the above models.

2.1.1. Combined+3 model

The "Combined+3 model", first used by the authors in Refs. [1–3], was formed by including three additional terms $1/s^2$, $1/s^3$ and $1/s^4$ to the existing combined model. These terms are introduced to capture the sharp decline (or "knee") in the OCV as the SOC reaches zero. It is noticed that, such sharp knees are found in the majority of the batteries except for a few battery chemistries. For batteries without such knee shape in the OCV–SOC characterization, the Combined model alone will be adequate to accurately capture the OCV curve.

2.1.2. Chebyshev model

The Chebyshev model is proposed in this paper due to its numerically stable characteristics in fixed point implementations

and its known property of minimizing the maximum error (i.e., uniform error across all SOC values) [22,23].

Let us define $s_c \in [-1,1]$ as

$$s_c = 2s - 1 \tag{5}$$

The function $V_o(s)$ can be approximated in terms of the Chebyshev polynomial as

$$V_o(s) \approx \sum_{i=0}^{L-1} K_i T_i(\bar{s}_{ck}) \tag{6}$$

where

$$K_0 = \frac{1}{L}\sum_{k=1}^{L} V_o(\bar{s}_{ck}) \tag{7}$$

$$K_i = \frac{2}{L}\sum_{k=1}^{L} V_o(\bar{s}_{ck}) T_i(\bar{s}_{ck}) \tag{8}$$

and

$$\bar{s}_{ck} = \cos\frac{\pi(2k-1)}{2L}, \quad k = 1,2,\ldots,L \tag{9}$$

$$T_i(\bar{s}_{ck}) = \cos\frac{i(2k-1)\pi}{2L}, \quad i < L \tag{10}$$

2.1.3. Clenshaw recurrence for the evaluation of Chebyshev model

Once the coefficients of the Chebyshev expansion are known, then $V_o(s)$ for any given $s \in [0,1]$ can be computed using the backward recurrence relations

$$y_{L+1} = 0 \tag{11}$$

$$y_L = 0 \tag{12}$$

$$y_{L-1} = K_{L-1} - y_{L+1} + 2y_L s_c \tag{13}$$

$$\vdots$$

$$y_1 = K_1 - y_3 + 2y_2 s_c \tag{14}$$

$$y_0 = K_0 - y_2 + 2y_1 s_c \tag{15}$$

$$V_o(s) = (K_0 - y_2) + y_1 s_c = y_0 - y_1 s_c \tag{16}$$

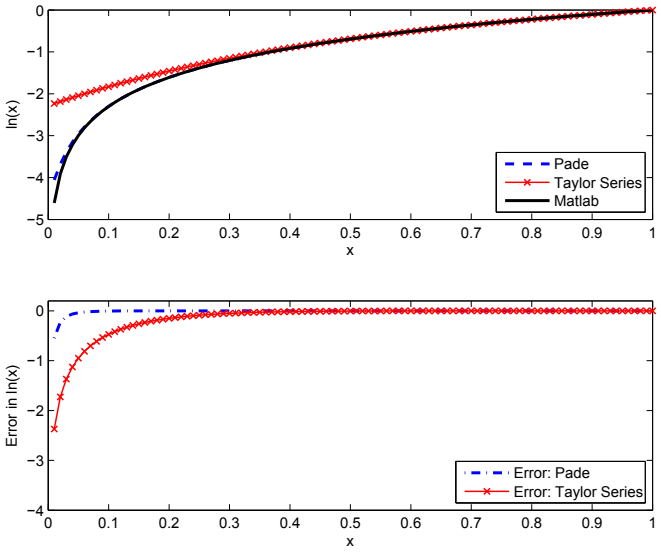

Fig. 3. Computing ln through Padé approximation. Top plot shows ln(x) computed by Padé approximation (18), Taylor series approximation and Matlab (version 2011b). The error plots in the bottom are relative to the Matlab version.

This numerically stable approach to the evaluation of functions expressed in Chebyshev series is known as Clenshaw's recurrence.

2.1.4. Padé approximation of natural logarithm

For OCV–SOC models that include natural logarithm, there needs to be an approximate way to implement them in smaller micro controllers and hardware logic circuits. We use the following expression, which gives a very accurate approximation of natural logarithm through Padé approximation [24]

$$\ln_{pade}(1-x) = \frac{0.01812x^5 - 0.30555x^4 - 1.30555x^3 - 2x^2 + x}{0.00396x^5 - 0.11904x^4 + 0.83333x^3 - 2.22222x^2 + 2.5x - 1} \tag{17}$$

The $\ln_{pade}$ above can be implemented efficiently using Horner's method as follows:

$$\ln_{pade}(1-x) = \frac{((((137x - 2310)x + 9870)x - 15120)x + 7560)x}{((((30x - 900)x - 6300)x - 16800)x + 18900)x - 7560} \tag{18}$$

In Fig. 3, the $\ln_{pade}$ approximation is compared with ln implemented using 5th order Taylor series approximation and the ln implementation by Matlab. It shows that the Padé approximation is more accurate than Taylor series approximation of the same order.[5]

[5] Indeed, higher order Taylor series approximations, up to more than 15th order, were tested and the conclusion is that the Taylor series approximation did not improve the accuracy with respect to (18).

2.2. Nonlinear regression-based models

In this section, we review three non-linear models presented in the literature and present a new non-linear OCV–SOC model using a rational approximant.

For nonlinear modeling, we designate

$$V_{o,n}(s,\boldsymbol{\kappa}_o) \triangleq V_o(s) \tag{19}$$

where

$$\boldsymbol{\kappa}_o = [\kappa_0\ \kappa_1 \ldots \kappa_M] \tag{20}$$

is the nonlinear OCV parameter vector [25,27].

$$V_{o,n}(s,\boldsymbol{\kappa}_o) = \begin{cases} \kappa_0 + \kappa_1 s + \kappa_2\left(1 - e^{-\kappa_3 s}\right) + \kappa_4\left(1 - e^{-\frac{\kappa_5}{1-s}}\right) & \text{(a) Double exponential model [25]} \\ \kappa_0 - \dfrac{\kappa_1}{s} + \kappa_2 e^{-\kappa_3(1-s)} & \text{(b) Nonlinear exponential model 1 [26]} \\ \kappa_0 e^{-\kappa_1 s} + \kappa_2 + \kappa_3 s + \kappa_4 s^2 + \kappa_5 s^3 & \text{(c) Nonlinear exponential model 2 [27]} \\ \dfrac{\sum_{i=0}^{m} \kappa_i s^i}{1 + \sum_{j=1}^{n} \kappa_{j+m} s^j},\ m \geq 0, n > 0 & \text{(e) Rational approximant} \end{cases} \tag{21}$$

Rational Approximant: In (21), we propose a model based on rational approximant which gives very good modeling accuracy. The model based on rational approximant is proposed based on Padé approximation ideas of [24]. The coefficients $\kappa_0, \kappa_1, \ldots, \kappa_{m+n}$ of the rational approximant can be uniquely determined. This method is also known as m/n order rational approximant.

2.3. Hybrid or piecewise linear models

It was noticed that using a single function to model the entire shape of $V_\circ(s)$ requires more parameters to reach a certain accuracy. The same level of accuracy can be obtained with fewer parameters through hybrid modeling. The objective is to simplify the models as much as possible, hence, only linear regression-based models are considered in this approach.

The intuition behind hybrid modeling is to approximate the OCV models as a few linear curves. For example, for some batteries, starting from a fully charged state, the OCV decreases gradually (and linearly) with SOC until a certain (low) SOC. After that, the OCV drops steeply (and linearly) with decreasing SOC. This particular battery can be represented using two straight lines: one for the gradual drop and the other for the steep drop. Some other OCV–SOC characteristic curves could be approximated by three (or more) different models. We consider only two of the following general form:

$$V_\circ(s) = \begin{cases} \mathbf{p}^i_\circ(s)^T \mathbf{k}^i_\circ & \text{if } s \geq \zeta \\ \mathbf{p}^j_\circ(s)^T \mathbf{k}^j_\circ & \text{if } s < \zeta \end{cases} \tag{22}$$

where each of $\mathbf{p}^i_\circ(s)$ and $\mathbf{p}^j_\circ(s)$ denote one of the eight different OCV models in (3). In this paper, we chose the combined model for $\mathbf{p}^i_\circ(s)$ and a 2nd order polynomial model for $\mathbf{p}^j_\circ(s)$. It is possible to have $i = j$ with the exception that the corresponding parameters $\mathbf{k}^i_\circ$ and $\mathbf{k}^j_\circ$ respectively, have to be different.

When $\mathbf{p}^i_\circ(s)$ and $\mathbf{p}^j_\circ(s)$ represent two straight lines, the minimum number of parameters will be five: two parameters each for the straight lines and ζ.

2.4. OCV–SOC table

An alternate approach to OCV modeling is to store values of OCV and SOC as a table. Table 1 shows such an OCV–SOC table made of 11 SOC points. It will become apparent after Section 4 that, only one OCV–SOC table is all that is required for fuel gauging at all temperatures. Generally, the BFG algorithm requires the derivative of the OCV function to be used in an extended Kalman filter-based SOC tracking approach; hence, the table needs to store the derivatives as well.

Table 1 was formed by uniformly sampling SOC. A nonlinear sampling can be employed for better accuracy. For example, selecting the number of samples in a "region" proportional to $dV_\circ(s)/ds$ will be more accurate than a table made of samples selected linearly across $s \in [0,1]$.

3. OCV parameter estimation techniques

In this section, we describe approaches for estimating the parameters of the models described in Section 2. For accurate estimation, we need the $\{V_\circ(s),s\}$ pairs spanning $s \in [0,1]$. We collect this data by discharging the battery from full-to-empty and then charging it back from empty-to-full with a very low current (C/30 to C/40).[6]

Fig. 4 shows the equivalent circuit of a battery when it is charged/discharged with a constant rate. First, we define the SOC at a given time as

$$s\left[t_k\right] \triangleq s \quad \text{at time } t_k \tag{23}$$

Considering the voltage measurement errors, the measured voltage is written as

$$z_v[t_k] = v[t_k] + n_v[t_k] \tag{24}$$

where $n_v[t_k]$ is the voltage measurement noise which is modeled as white Gaussian with standard deviation (s.d.) σ_v. Since the current during the OCV experiment is usually kept constant through highly accurate programmable charge/load devices, we assume that there is no noise involved in $i[t_k]$.

[6] C/N is a common representation for the discharge/charge rate of a battery, where C denotes the battery capacity in Ah and N is in hours.

Table 1
A sample OCV–SOC table that requires 11 memory space.

s	$V_\circ(s)$	$dV_\circ(s)/ds$
0.0	3.0519	44.4073
0.1	3.6594	0.6830
0.2	3.7167	0.8131
0.3	3.7611	0.4807
0.4	3.7915	0.4393
0.5	3.8275	0.6055
0.6	3.8772	0.8113
0.7	3.9401	0.9777
0.8	4.0128	1.0915
0.9	4.0923	1.1822
1.0	4.1797	1.3405

During the OCV experiment, the terminal voltage can be written as

$$z_v[t_k] = V_\circ(s[t_k]) + h[t_k] + i[t_k]R_0 + n_v[t_k] \tag{25}$$

where $h[t_k]$ is the hysteresis or voltage "pull" which is a function of current and SOC of the battery. Since the OCV test is performed at a very low current, we assume that the hysteresis is proportional to the current only, i.e.

$$h[t_k] \propto i[t_k] \tag{26}$$

Hence, (25) can be rewritten as

$$z_v[t_k] = V_\circ(s[t_k]) + i[t_k]R_{0,h} + n_v[t_k] \tag{27}$$

where the *effective resistance*

$$R_{0,h} = R_0 + R_h \tag{28}$$

is the summation of the battery series resistance R_0 and the *constant-current hysteresis equivalent resistance*, R_h.

3.1. Linear model parameter estimation

The parameters of the linear OCV–SOC model in (2) can be written as,

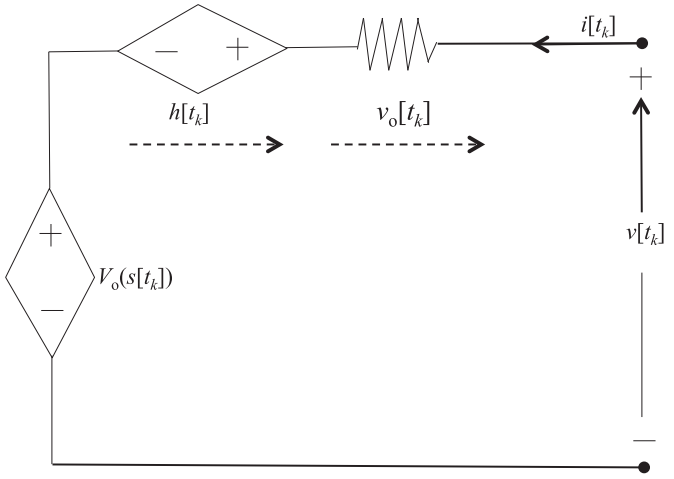

Fig. 4. Equivalent circuit of a battery when it experiences constant current. When the current is constant for a long time, the internal capacitors of the battery becomes saturated and the battery equivalent circuit becomes just a resistor.

$$z_v\begin{bmatrix} t_k \end{bmatrix} = \underbrace{\begin{bmatrix}\mathbf{p}_\circ(s[t_k])^T & i\begin{bmatrix}t_k\end{bmatrix}\end{bmatrix}}_{\mathbf{p}[t_k]^T} \underbrace{\begin{bmatrix}\mathbf{k}_\circ \\ R_{0,h}\end{bmatrix}}_{\mathbf{k}} + n_v\begin{bmatrix} t_k \end{bmatrix} \tag{29}$$

By considering a batch of N voltage observations, (29) can be written as

$$\mathbf{v} = \mathbf{P}k + \mathbf{n} \tag{30}$$

where

$$\mathbf{v} = [v[t_1]\ v[t_2]\ldots v[t_N]]^T \tag{31}$$

$$\mathbf{p} = [\mathbf{p}[t_1]\ \mathbf{p}[t_2]\ldots\mathbf{p}[t_N]]^T \tag{32}$$

$$\mathbf{n} = [n[t_1]\ n[t_2]\ldots n[t_N]]^T \tag{33}$$

$$\mathbf{k} = [\mathbf{k}_\circ\ R_{0,h}]^T \text{an } (M+2)\text{vector} \tag{34}$$

The least squares estimate of the parameter vector is given by

$$\widehat{\mathbf{k}} = \left(\mathbf{p}^T\mathbf{p}\right)^{-1}\mathbf{p}^T\mathbf{v} \tag{35}$$

Now, for a given SOC s, the corresponding OCV estimate $\widehat{V}_\circ(s)$ is computed as

$$\widehat{V}_\circ(s) = \mathbf{p}_\circ(s)^T\widehat{\mathbf{k}} \tag{36}$$

where $\widehat{\mathbf{k}}$ is formed by the first $M+1$ (4) elements of $\widehat{\mathbf{k}}$.

In Fig. 5, the estimated values of $R_{0,h}$, R_0, and R_h are shown using data collected on a Samsung battery with serial number EB575152 at different temperatures. The average modeling error at each

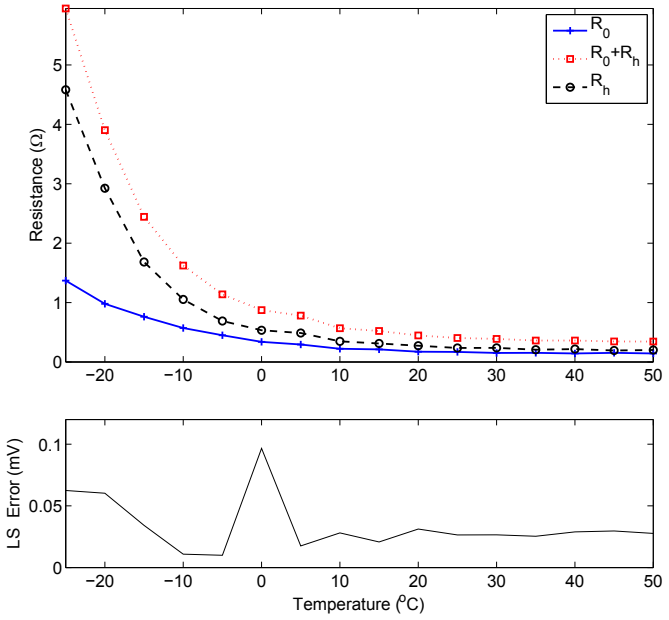

Fig. 5. Estimated resistance values. *Top*: the estimated value of effective resistance $R_{0,h} = R_0 + R_h$ is compared with the series resistance R_0, which was computed by applying a discharge pulse on the battery. The computed value of hysteresis equivalent resistance, $R_h = R_{0,h} - R_0$, is also plotted; R_h shows a similar temperature dependence as R_0. *Bottom*: corresponding modeling error relative to the voltage observations.

temperature is also shown in the bottom of the plot. The average modeling error is discussed later; briefly, the average modeling error is computed by averaging the voltage error for the entire range of SOC, for example, the error at 50 °C is computed by averaging the error shown in the bottom Fig. 17. The box plot in Fig. 18 shows this modeling error across multiple batteries and temperatures.

3.2. Total least squares parameter estimation

In contrast to the classical least squares (LS) problem, in which the solution to the linear system of equations $\mathbf{Pk} \approx \mathbf{v}$ assumes noise only in the observation vector $\mathbf{v}$, the total least squares (TLS) problem assumes that the elements of both $\mathbf{P}$ and $\mathbf{v}$ are contaminated by noise. This leads to the following formulation

$$\hat{\mathbf{k}}_{\mathrm{TLS}} = \arg\min_{\mathbf{k},\hat{\mathbf{P}},\hat{\mathbf{v}}} \left|\left| \left[\mathbf{p}\ \mathbf{v}\right] - \left[\hat{\mathbf{P}}\ \hat{\mathbf{v}}\right] \right|\right|_F \tag{37}$$

subject to

$$\hat{\mathbf{P}}k = \hat{\mathbf{v}} \tag{38}$$

where $[\mathbf{P}\ \mathbf{v}]$ and $[\hat{\mathbf{P}}\ \hat{\mathbf{v}}]$ are matrices of equal size. The matrix $\mathbf{P}$ is noisy due to errors in computed SOC, as discussed in Section 4.

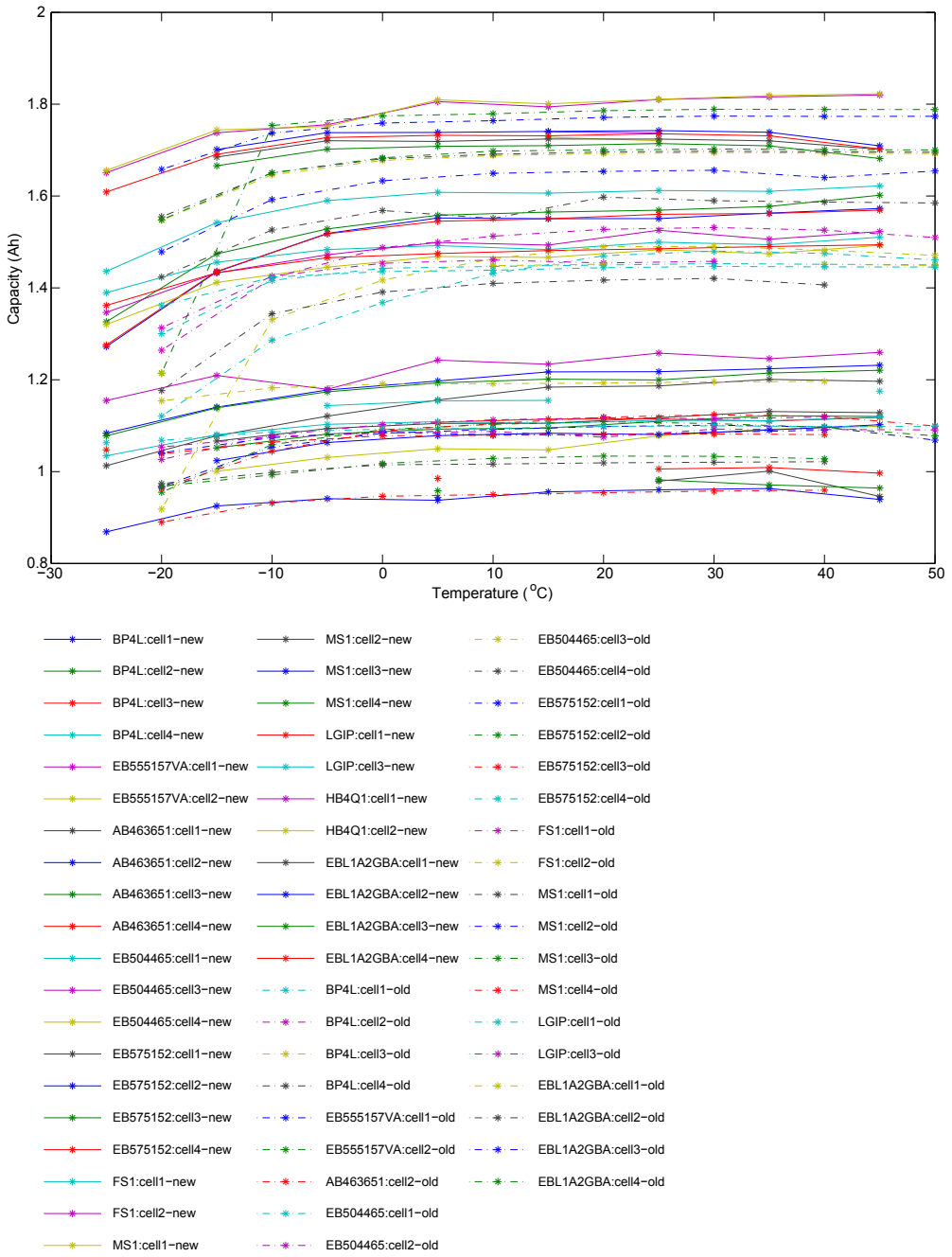

Fig. 6. Estimated battery capacities at different temperatures. The capacities are computed by C/30 discharge. Capacity measurements from 34 battery cells are plotted against temperature. Markers indicate the measurement and the lines connect the measurements that correspond to a certain cell. Details from each cells are shown in Figs. 7–10 for clarity.

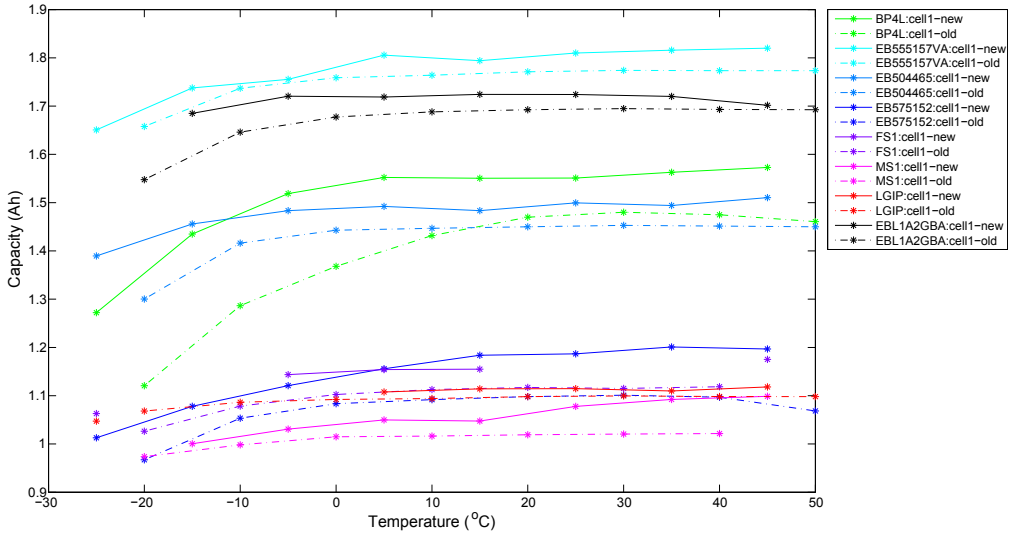

Fig. 7. New vs. old battery capacity against temperature. Only cell 1 data from Fig. 6 is shown.

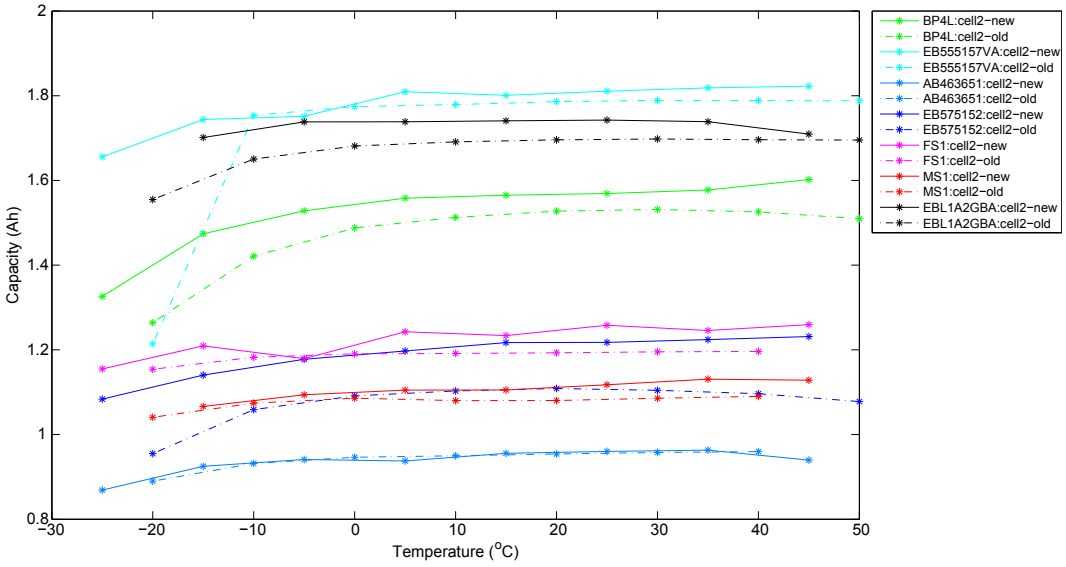

Fig. 8. New vs. old battery capacity against temperature. Only cell 2 data from Fig. 6 is shown.

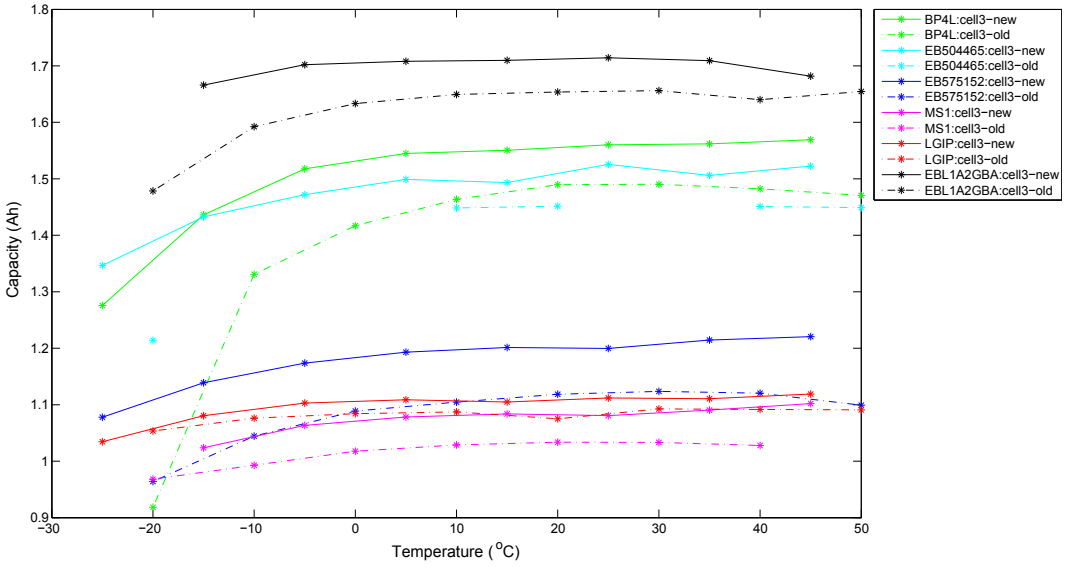

Fig. 9. New vs. old battery capacity against temperature. Only cell 3 data from Fig. 6 is shown.

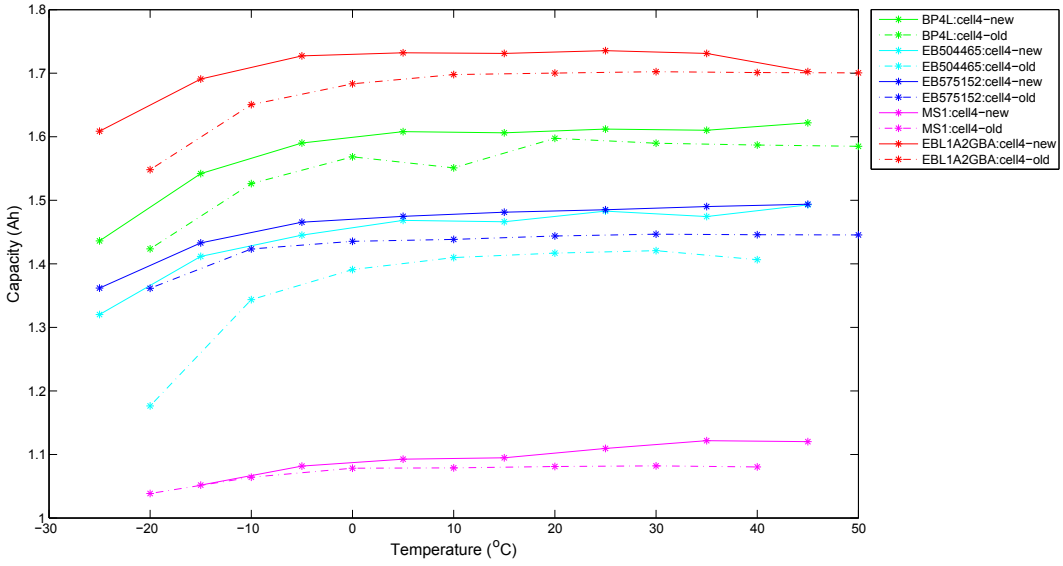

Fig. 10. New vs. old battery capacity against temperature. Only cell 4 data from Fig. 6 is shown.

Further discussion of the TLS approach and its method of solution can be found in Refs. [28–30].

3.3. Nonlinear model parameter estimation

For nonlinear models, we rewrite (39) in the following form

$$\mathbf{v}(\boldsymbol{\kappa}) = \mathbf{v}_\circ(\boldsymbol{\kappa}_\circ) + \mathbf{i}R_{0,h} + \mathbf{w} \tag{39}$$

where

$$\boldsymbol{\kappa} = \left[\boldsymbol{\kappa}_\circ \; R_{0,h}\right]^T \tag{40}$$

$$\mathbf{v}_\circ(\boldsymbol{\kappa}_\circ) = \left[V_{\circ,n}(s[t_1], \boldsymbol{\kappa}_\circ) \ldots V_{\circ,n}(s[t_N], \boldsymbol{\kappa}_\circ)\right]^T \tag{41}$$

$$\mathbf{i} = [i[t_1]\; i[t_2] \ldots, i[t_N]] \tag{42}$$

and $\mathbf{w}$ is the noise vector.

The coefficients of the nonlinear regression-based models were computed using the Matlab optimization toolbox function for nonlinear least squares *lsqnonlin*. The nonlinear least squares problem solves the following problem

$$\widehat{\boldsymbol{\kappa}} = \arg\min_{\boldsymbol{\kappa}} ||\mathbf{v} - \widehat{\mathbf{v}}(\boldsymbol{\kappa})|| \tag{43}$$

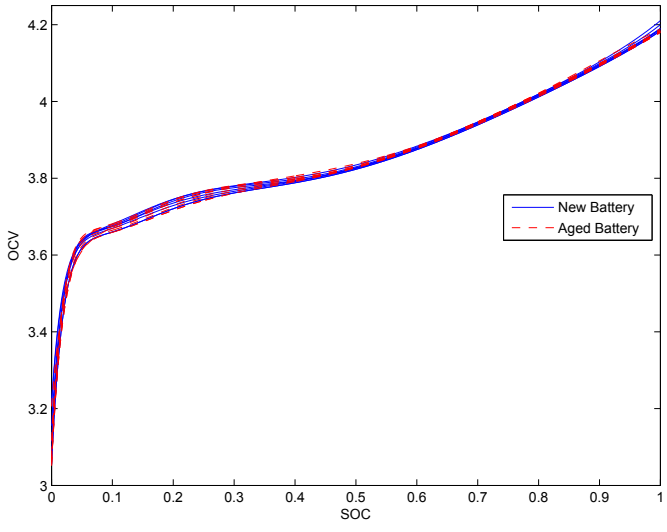

Fig. 11. OCV–SOC characterization curves of new vs. aged batteries. New battery curves are plotted in solid blue and aged battery curves are plotted in dashed red. Different curves of the same type correspond to temperatures ranging from −25 °C to 50 °C. The new and aged battery OCV curves overlap. (For interpretation of the references to color in this figure legend, the reader is referred to the web version of this article.)

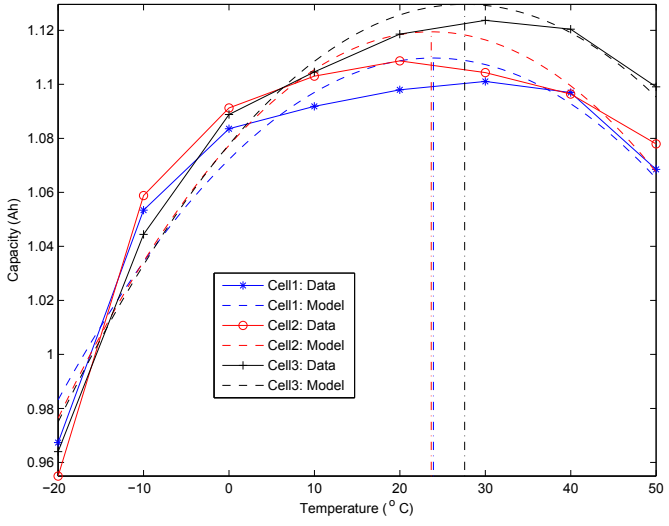

Fig. 12. A quadratic model fitting on total capacity estimates: Each measurement plot in Fig. 6 is fitted with a quadratic model. Here we demonstrate quadrature model fitting on 3 different cells of the same chemistry and type. The corresponding model capacity is plotted in dashed line of the same color. The estimated nominal temperature (60) $\widehat{T}_{\text{nom}}$ that corresponds to the maximum capacity is shown in dash-dot line of the same color. (For interpretation of the references to color in this figure legend, the reader is referred to the web version of this article.)

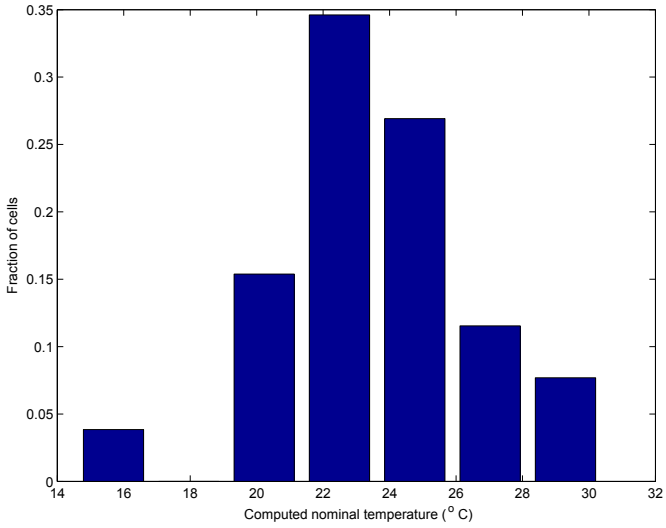

Fig. 13. Analysis of estimated nominal temperature: estimated nominal temperature of 34 battery cells of different manufacturers is used for this experiment.

3.4. Hybrid model parameter estimation

It is well known that OCV is a monotonically increasing function of SOC. Consequently, we imposed the inequality constraint $dV_\circ(s)/ds \geq 0$ in order to obtain an OCV model with monotonic estimates of OCV with respect to SOC.

Furthermore, in hybrid models, the OCV model is assumed to follow a particular function until $s = \zeta$ and then assumes a different model structure. In order to realize such a model structure, the least squares problem is implemented with additional equality constraints as shown below:

$$\widehat{\mathbf{k}}_1 = \arg\min_{\mathbf{k}_1} \left\| \left(\mathbf{p}^i(s)\mathbf{k}_1 - \mathbf{v} \right) \right\| \quad s \in [0, \zeta] \tag{44}$$

subject to

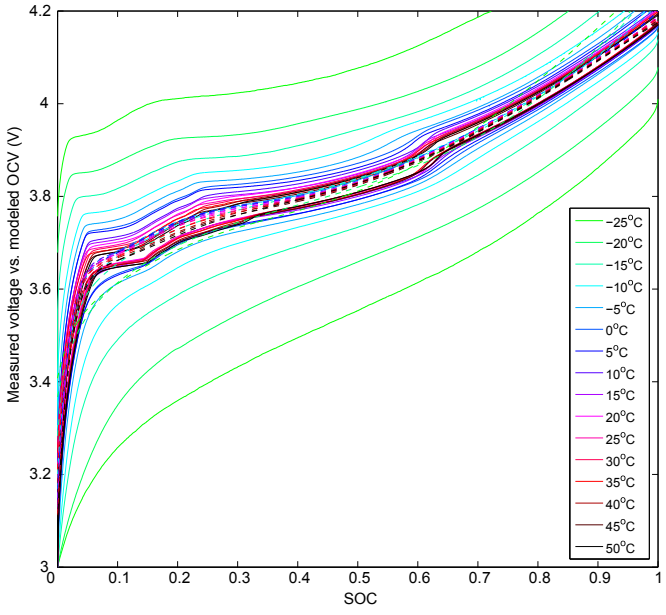

Fig. 14. Normalized OCV modeling. Measured terminal voltage is shown in solid and computed OCV is shown in dashed lines. The solid lines show the measured voltage and the dashed lines show the normalized OCV curves; the normalized OCV curves nearly coincide for all temperatures.

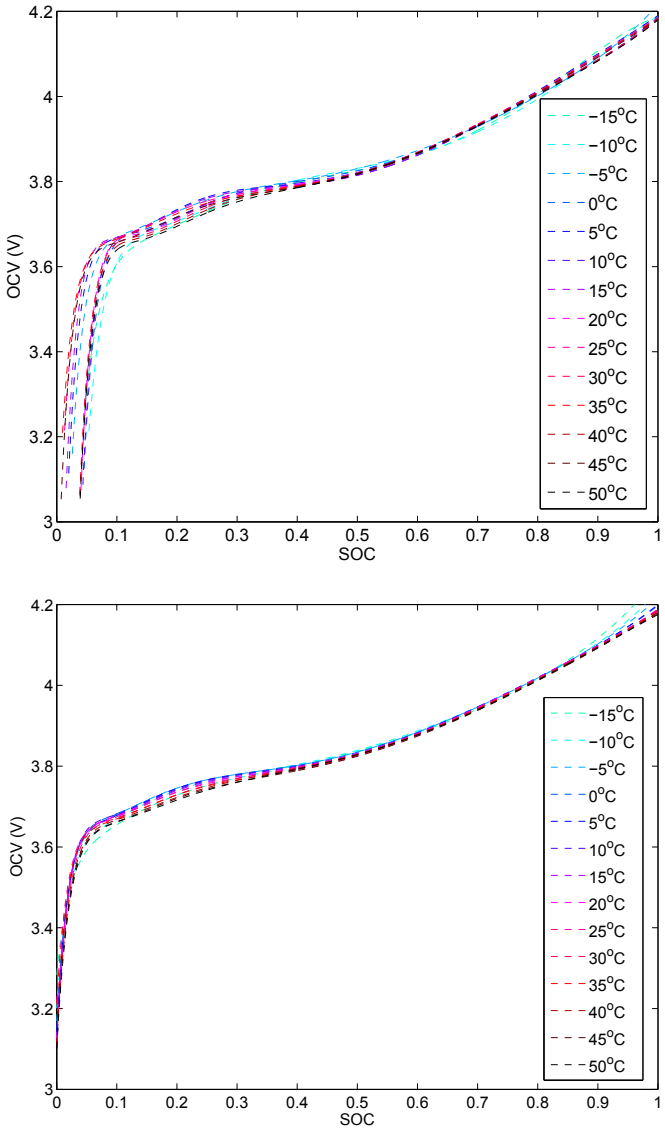

Fig. 15. Nominal vs. normalized OCV modeling. *Top*: nominal OCV modeling uses $C_{\text{nom}} = 1.5$ Ah in computing SOC at all temperatures. *Bottom*: normalized OCV modeling computes C_{batt} at each temperature before computing SOC.

$$\frac{d\mathbf{p}^i\widehat{\mathbf{k}}_1}{ds} > 0 \tag{45}$$

$$\mathbf{p}^i(s)\widehat{\mathbf{k}}_1\Big|_{s=\zeta} - \mathbf{p}^j(s)\widehat{\mathbf{k}}_2\Big|_{s=\zeta} = 0 \tag{46}$$

$$\frac{d\mathbf{p}^i(s)\widehat{\mathbf{k}}_1}{ds}\Big|_{s=\zeta} - \frac{d\mathbf{p}^j(s)\widehat{\mathbf{k}}_2}{ds}\Big|_{s=\zeta} = 0 \tag{47}$$

$$\frac{d^2\mathbf{p}^i(s)\widehat{\mathbf{k}}_1}{ds^2}\Big|_{s=\zeta} - \frac{d^2\mathbf{p}^j(s)\widehat{\mathbf{k}}_2}{ds^2}\Big|_{s=\zeta} = 0 \tag{48}$$

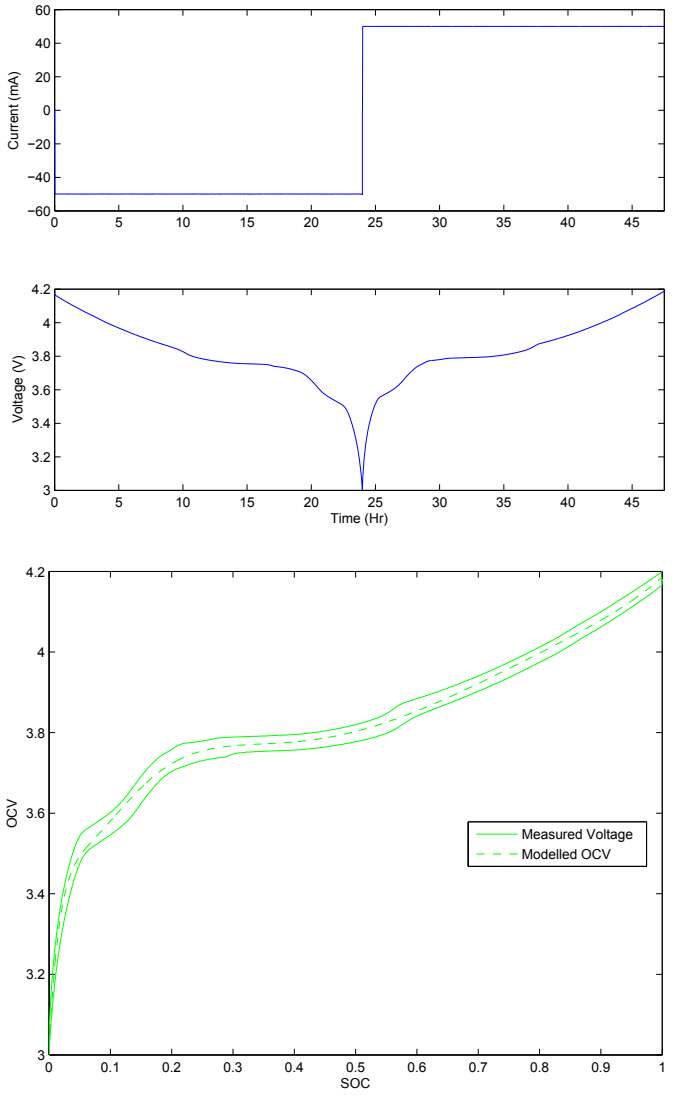

Fig. 16. OCV–SOC characterization data and sample OCV plot. Top two plots indicate the applied current $i[t_k]$ and measured voltage $z_v[t_k]$. The plot at the bottom shows the same $z_v[t_k]$ in the middle plot above against SOC, instead of time. The SOC was computed by Coulomb counting, explained later in (54). The OCV is computed using (36).

$$\widehat{\mathbf{k}}_2 = \arg\min_{\mathbf{k}_2} \left\| \left(\mathbf{p}^j(s)\mathbf{k}_2 - \mathbf{v} \right) \right\| \quad s \in (\zeta, 1] \tag{49}$$

subject to

$$\frac{\mathrm{d}\mathbf{p}^j \widehat{\mathbf{k}}_2}{\mathrm{d}s} > 0 \tag{50}$$

$$\mathbf{p}^i(s)\widehat{\mathbf{k}}_1\Big|_{s=\zeta} - \mathbf{p}^j(s)\widehat{\mathbf{k}}_2\Big|_{s=\zeta} = 0 \tag{51}$$

$$\frac{\mathrm{d}\mathbf{p}^i(s)\widehat{\mathbf{k}}_1}{\mathrm{d}s}\Big|_{s=\zeta} - \frac{\mathrm{d}\mathbf{p}^j(s)\widehat{\mathbf{k}}_2}{\mathrm{d}s}\Big|_{s=\zeta} = 0 \tag{52}$$

$$\frac{\mathrm{d}^2\mathbf{p}^i(s)\widehat{\mathbf{k}}_1}{\mathrm{d}s^2}\Big|_{s=\zeta} - \frac{\mathrm{d}^2\mathbf{p}^j(s)\widehat{\mathbf{k}}_2}{\mathrm{d}s^2}\Big|_{s=\zeta} = 0 \tag{53}$$

The constrained least squares algorithm software in the optimization toolbox of Matlab is used for the optimizations above.

4. Normalized OCV modeling

So far in OCV model parameter estimation the SOC is assumed to be known, for example, the SOC in (27) is computed through Coulomb counting:

$$s\left[t_k\right] = s\left[t_{k-1}\right] + \frac{\eta\Delta_k}{3600C}\left(\frac{i[t_{k-1}] + i[t_k]}{2}\right) \tag{54}$$

where

$$\Delta_k = t_k - t_{k-1} \tag{55}$$

is the sampling interval, and

$$\eta = \begin{cases} \eta_c \leq 1 & \text{during charging} \\ \eta_d = 1 & \text{during discharging} \end{cases} \tag{56}$$

is the efficiency and C denotes the battery capacity (in Ampere-hours), which plays a major role in OCV-SOC characterization of the battery, as we describe below.

There are two different ways of characterizing OCV based on the assumption of the battery capacity:

$$C = \begin{cases} C_{\text{nom}} & \text{Nominal OCV modeling} \\ C_{\text{batt}} & \text{Normalized OCV modeling} \end{cases} \tag{57}$$

where C_{batt} is the total battery capacity (clearly defined in a subsequent paragraph).

We define

1. *Nominal OCV modeling*, when the same battery capacity $C = C_{\text{nom}}$ is used at all temperatures for computing the SOC in (27) and
2. *Normalized OCV modeling*, when the computed total battery capacity $C = C_{\text{batt}}$ at each temperature is used for computing the SOC in (27).

In Fig. 6, we show the total capacities, computed by C/30 discharge from full to empty, of cells listed in Table 2 at different temperatures. All the batteries are purchased through commercial vendors; the manufacturer data sheets were not available to any of the batteries. The chemical composition of the batteries was learned through destructive analysis on sample batteries. All the Samsung cells were found to be of $LiCoO_2$ cathode, Carbon anode systems, with carbonate-based electrolytes containing $LiPF_6$ as the primary salt. The capacity vs. temperature is observed to take a concave form in general, i.e., the maximum total capacity is achievable only at a particular temperature.

Now, let us define the following terms related to battery capacity:

- **Maximum/full-charge battery open circuit voltage** (OCV_{max}): OCV_{max} refers to the OCV of the battery when it is fully charged, i.e.,

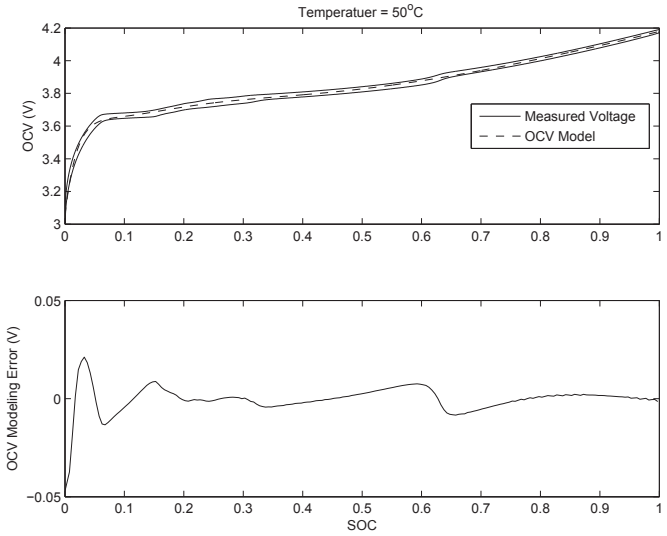

Fig. 17. Sample OCV modeling error. *Top*: Measured voltage and modeled OCV. *Bottom*: OCV modeling error.

$$\mathrm{OCV}_{\max} = V_{\circ}(s)|_{s=1} \tag{58}$$

It must be noted that due to the internal impedance of the battery and hysteresis, the measured cell voltage of the battery will be higher than $\mathrm{OCV}_{\max}$ right after the battery is fully charged.

- **Minimum/empty battery open circuit voltage** ($\mathrm{OCV}_{\min}$): Similar to (58)

$$\mathrm{OCV}_{\min} = V_{\circ}(s)|_{s=0} \tag{59}$$

where, due to the internal impedance of the battery and hysteresis, the measured cell voltage of the battery will be lower than $\mathrm{OCV}_{\min}$ right after the battery is fully discharged.

- **Rated battery capacity**, C_r: Rated capacity is the manufacturer specified (labeled) capacity of the battery. Manufacturer specified capacity should be treated as an approximate measure of the true value of battery capacity at the specified temperature.
- **Total capacity**, C_{batt} or $C_{\mathrm{batt}}(T)$: Total battery capacity is the maximum amount of Coulombs that can be discharged from a battery at cell temperature T, starting from a fully charged battery corresponding to its $\mathrm{OCV} = \mathrm{OCV}_{\max}$ until the battery is fully discharged, i.e., until the battery terminal reaches $\mathrm{OCV} = \mathrm{OCV}_{\min}$ using an infinitesimal[7] load current.
- **Nominal capacity**,[8] C_{nom}: Nominal capacity is the maximum amount of Coulombs that can be discharged from a battery at any cell temperature. In other words, nominal capacity is the maximum total capacity of the battery. The temperature at which the total battery capacity is maximum is defined as the **nominal temperature** of the battery, i.e.,

$$\widehat{T}_{\mathrm{nom}} = \arg\max_{T} C_{\mathrm{batt}}(T) \tag{60}$$

$$C_{\mathrm{nom}} = C_{\mathrm{batt}}\left(\widehat{T}_{\mathrm{nom}}\right) \tag{61}$$

The total capacity C_{batt} increases with temperature up to the nominal temperature. Beyond that, the total capacity starts to decline with increasing temperature. The above definition implies that the nominal temperature of the battery varies from battery to battery. It must be noted that the manufacturer specified nominal temperature (and nominal capacity) are only approximate. Hence, for accurate BFG, the nominal temperature of the battery must be dynamically estimated — we will present those details in a future publication.

Table 3 lists the differences between nominal and normalized OCV modeling.

The conclusion is that the normalized OCV modeling has many advantages over nominal OCV modeling.

Fig. 12 shows the quadratic model fitting of the total capacity estimates against temperature using data collected from 3 different cells of the same chemistry and type of battery. Once the model is fitted, the nominal temperature and nominal capacity of the battery can be estimated based on (60) and (61).

The nominal temperatures are estimated for all the cells listed in Table 2 and Fig. 13 summaries the estimated nominal temperatures as a histogram. Based on these (limited number of) observations, the most cells had a nominal temperature of 22.5 °C and the average nominal temperature is 23.5 °C. It must be noted that in most of the batteries in Table 2, the manufacturer specified nominal temperature is 25 °C. Hence, for superior accuracy, a BFG must estimate (and track) the Capacity of the battery.

Fig. 14 shows an example of normalized OCV modeling at different temperatures. It can be seen that regardless of the measured terminal voltages at different temperatures, the corresponding OCV curves are nearly identical. This is further illustrated later, using Fig. 15.

Fig. 15 shows the comparison of OCV–SOC curves obtained from nominal (top) and normalized (bottom) OCV–SOC characterization. The nominal OCV modeling used $C_{\mathrm{nom}} = 1.5$ Ah in computing SOC at all temperatures and the normalized modeling used the computed total capacity at each temperature in order to compute SOC. It can be observed that in normalized OCV modeling, the curves computed at all temperatures are nearly identical.

Fig. 11 shows the OCV–SOC characteristic curves, obtained on a new as well as aged battery at different temperatures. First, the OCV data was collected from a newly bought battery at −25 °C, −15 °C, −5 °C, 15 °C, 25 °C and 35 °C and 45 °C. Then, the battery was left for "self aging" for approximately one year. Then, the OCV data was collected from this aged battery at −20 °C, −10 °C, 0 °C, 10 °C, 20 °C and 30 °C, 40 °C and 50 °C.[9] It can be seen that no significant difference of patterns was found with respect to the age and temperature of the battery. Consequently, a single normalized OCV–SOC curve in conjunction with an adaptive battery capacity estimation algorithm can be used in

[7] The series resistance of the battery prevents measured terminal voltage from reaching $\mathrm{OCV}_{\min}$ and hence fully discharging the battery. A smaller load current makes sure the battery is fully emptied as much as possible. The gradient of the OCV–SOC curve is very high (see Table 1 and a sample OCV–SOC plot in Fig. 11) close to an empty battery, which helps minimize the errors in total capacity estimation by slow discharging.

[8] Most of the battery literature treats nominal capacity as exactly similar to the rated capacity. We introduce this slightly altered definition based on observations in the literature where the nominal capacity is treated as the maximum possible capacity. For example, in Ref. [31], the nominal capacity of a power plant is the maximum possible power output. Nominal capacity is technically achievable, but, not always practical. In the battery example, the nominal capacity is only achievable at the nominal temperature.

[9] There was no particular reasons for the selection of these temperatures. At first, it was decided to do the tests in 10 °C intervals and later it was decided to the tests (on aged batteries) at slightly different temperature.

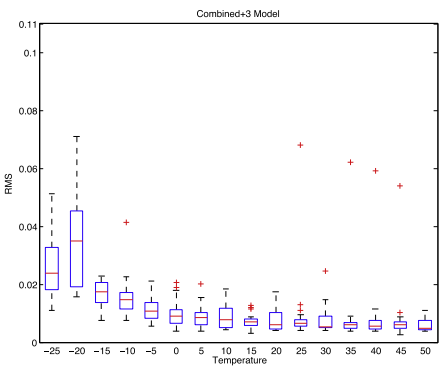

(a) Combined+3

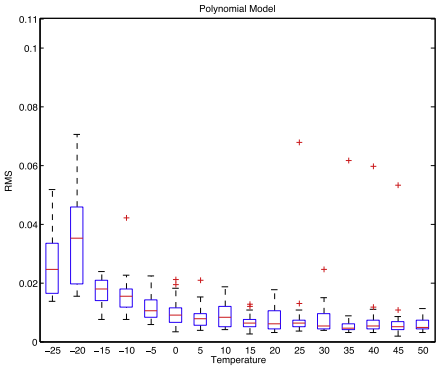

(b) Polynomial

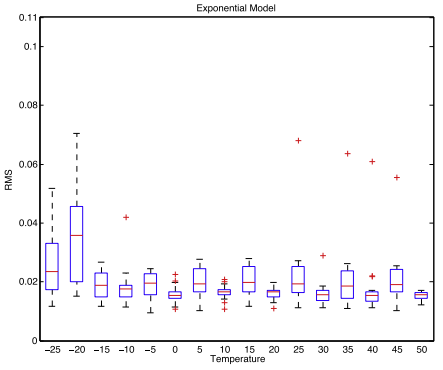

(c) Exponential

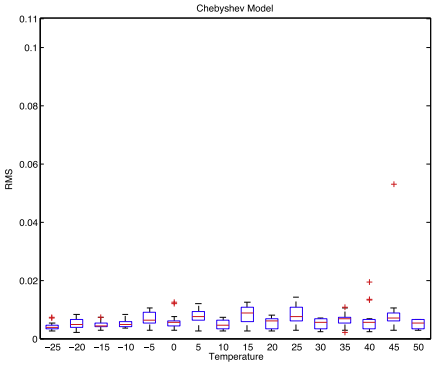

(d) Chebyshev

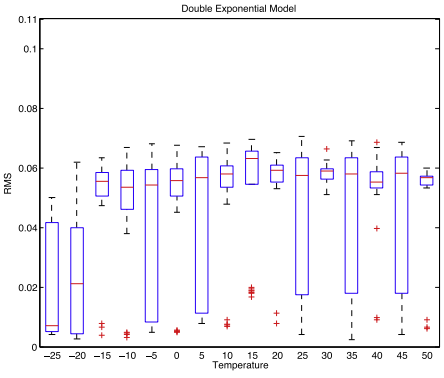

(e) Double Exponential

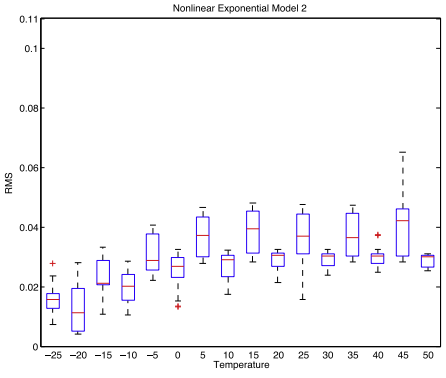

(f) Nonlinear Exponential 2

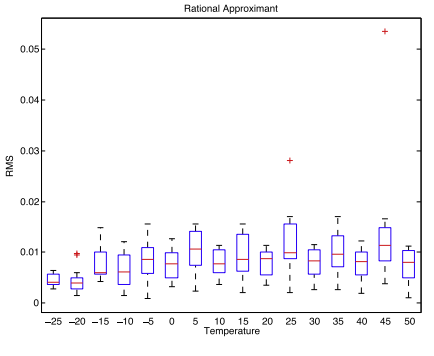

(g) Rational Approximant

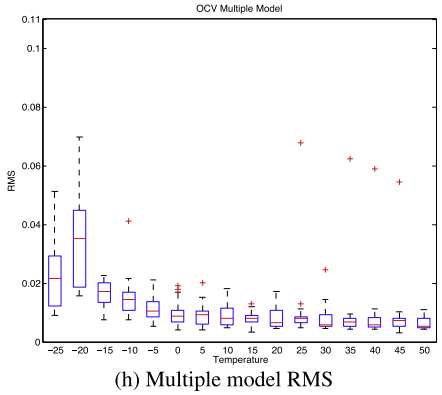

(h) Multiple model RMS

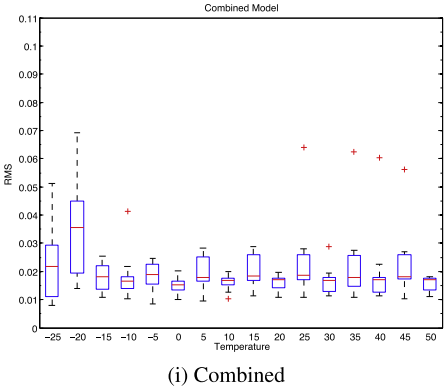

(i) Combined

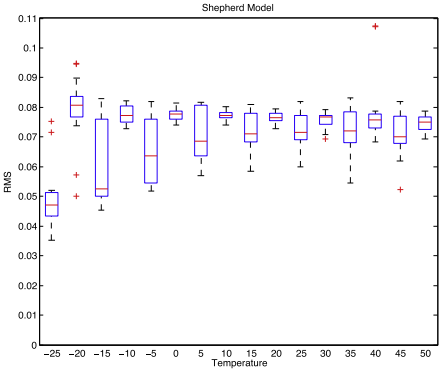

(j) Shepherd

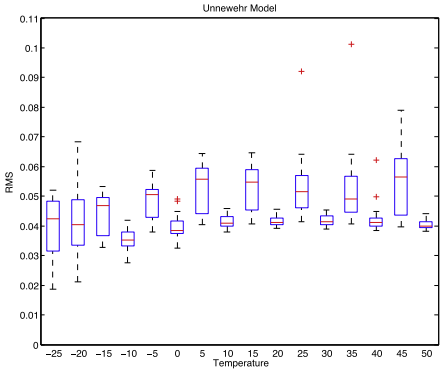

(k) Unnewehr

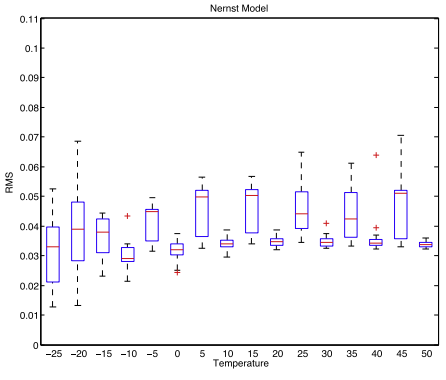

(l) Nernst

Fig. 18. RMS error across different battery cells. RMS value of the OCV modeling error across different battery cells is given as a box plot (the central (red) mark of the box is median; the edges of the box are 25th and 75th percentile values; the whiskers extend to the most extreme data points not considered outliers, and outliers are plotted individually with a '+') at each temperature. (For interpretation of the references to color in this figure legend, the reader is referred to the web version of this article.)

Table 2
Hardware-in-the-loop battery OCV–SOC characterization data overview.

Battery Supplier	Battery type	Number of batteries	Rated capacity (mAh)
Samsung	EB575152VA	4	1500
Samsung	EBL1A2GBA	4	1650
Samsung	EB555157VA	2	1750
Samsung	EB504465VA	4	1500
Samsung	AB463651	4	960
Samsung	L1G6LLAGS	2	2100
Nokia	BP-4L	4	1500
LG	LGIP-530B	2	1100
RIM	F-S1	2	1270
RIM	M-S1	4	1500
Huawei	HB4Q1	2	1670

the BFG to obtain accurate SOC estimates for varying usage conditions over the lifetime of a battery.

5. OCV–SOC model metrics for selection of the best model

In this section, we develop a systematic approach to select the best approach for OCV models. This is done by computing several *error metrics* and *model evaluation metrics*, described below, and then by ranking the models based on *Borda counts*.

5.1. OCV prediction error metrics

The following four error metrics are used for predicting $\mathbf{v}$, defined in (31) to evaluate the models:

5.1.1. Best fit

$$\mathrm{BF}(\%) = \left(1 - \frac{\|\widehat{\mathbf{v}} - \mathbf{v}\|}{\|\mathbf{v} - \overline{\mathbf{v}}\|}\right) \times 100 \tag{62}$$

5.1.2. R^2 fit

$$\begin{aligned} \mathrm{R}^2(\%) &= \left(1 - \frac{\|\widehat{\mathbf{v}} - \mathbf{v}\|^2}{\|\mathbf{v} - \overline{\mathbf{v}}\|^2}\right) \times 100 \\ &= \left(\frac{\|\widehat{\mathbf{v}} - \overline{\mathbf{v}}\|^2}{\|\mathbf{v} - \overline{\mathbf{v}}\|^2}\right) \times 100 \\ &= [\mathrm{BF}(2 - \mathrm{BF})] \times 100 \end{aligned} \tag{63}$$

5.1.3. Max error

$$\mathrm{ME} = \max_i \{|\mathbf{v}_i - \widehat{\mathbf{v}}_i|\} \tag{64}$$

Table 3
Comparison of nominal vs. normalized OCV modeling.

Nominal OCV modeling	Normalized OCV modeling
The SOC at any temperature is relative to the fixed, nominal capacity of the battery	The SOC is relative to the total capacity of the battery at the given temperature
There is no need to know the total capacity at a temperature in order to compute the SOC	Need to know the total capacity in order to compute SOC at a particular temperature
Gives accurate (durable) OCV parameters only with a new battery	OCV–SOC characterization can be done using an aged battery as well
Capacity estimation becomes erroneous with an aged battery	Capacity estimation works well even for an aged battery

5.1.4. Root-mean square (RMS) error

$$\mathrm{RMS} = \frac{\|\mathbf{v} - \widehat{\mathbf{v}}\|}{\sqrt{N - M}} \text{ or } \sqrt{\mathrm{MSE}} \tag{65}$$

where N is the number of data points, M is the number of parameters, $\widehat{\mathbf{v}}$ is the predicted value of $\mathbf{v}$ using the estimated parameters, for example, for linear models

$$\widehat{\mathbf{v}} = \mathbf{P}\widehat{\mathbf{k}} \tag{66}$$

and

$$\overline{\mathbf{v}} = \frac{1}{N}\sum_{i=1}^{N} \widehat{\mathbf{v}}(i) \tag{67}$$

5.2. Model evaluation metrics

Model evaluation metrics consider the trade off between the number of model parameters and the number of data points. The following four metrics are important ones.

5.2.1. Akaike's information criterion (AIC)

If the models are fitted using Least Squares, then [32] suggests the following analog of AIC:

$$\mathrm{AIC} = N\ln\left(\frac{S_2}{N}\right) + 2(M + 1) \tag{68}$$

where

$$S_2 = \sum_{i=1}^{N} \mathbf{e}_i^2 \tag{69}$$

with

$$\mathbf{e} = \mathbf{v} - \widehat{\mathbf{v}} \tag{70}$$

In the above S_2 is the sum of the squares of errors (SSE), $\mathbf{e}_i$ is the ith element of the residual vector $\mathbf{e}$ and M is the number of parameters in the OCV model. The better the model, the lower the AIC.

5.2.2. Akaike's information criterion 2 (AIC2)

A second version of AIC, given below, is useful when $N \gg M$

$$\mathrm{AIC2} = \ln\left[\mathscr{S}_f\left(1 + \frac{2p}{N}\right)\right] \tag{71}$$

where the loss function is defined as

$$\mathscr{S}_f = \frac{\mathbf{e}^T\mathbf{e}}{N} \tag{72}$$

5.2.3. Akaike's final prediction error (FPE)

$$\mathrm{FPE} = \mathscr{S}_f\left[\frac{1 + \frac{M}{N}}{1 - \frac{M}{N}}\right] \tag{73}$$

5.2.4. Bayesian information criterion (BIC)

The derivation of BIC assumes equal priors on each model and noninformative priors on the parameters, given each model. The goal of the BIC is to find the best (i.e. highest posterior probability) model for prediction.

$$\mathrm{BIC} = 2(L_N) + (M+1)\ln N \tag{74}$$

The negative log-likelihood given the pdf of the residuals (assuming normal or Gaussian) conditioned on the parameters $\mathbf{k}$ and the s.d. of residuals σ is given by

$$L_N = -\ln\{L(\mathbf{k};\mathbf{e})\} = \sum_{i=1}^{N}\left\{\left(\frac{\mathbf{e}_i^2}{2\sigma^2}\right) + 0.5\ln\left(2\pi\sigma^2\right)\right\} \tag{75}$$

where, L_N is the negative log-likelihood, L is the likelihood, $\mathbf{k}$ is the parameter vector which minimizes L_N, and σ is the s.d. of the residuals $\mathbf{e}$.

5.2.5. Minimum description length (MDL)

$$\mathrm{MDL} = \mathscr{L}_f\left[1 + \frac{M\ln N}{N}\right] \tag{76}$$

5.3. Combining rankings

The Borda count [33] is an easy, intuitively appealing, and powerful method for combining different rankings. In this paper, we use Borda's count method to combine the rankings of different model selection metrics. The Borda count is originally a voting method in which each voter gives a complete ranking of all possible alternatives. The highest ranked alternative or OCV Model (in an n-way vote) gets n votes (or points) and each subsequent alternative gets one less vote (i.e. number 2 gets $n-1$ votes and number 3 gets $n-2$ votes and so on). Then, for each alternative, all the votes (or points) are added up and the alternative (i.e. OCV Model) with the highest number of votes wins the election. The OCV Models are then ranked in descending order of votes (or points) to give the overall Borda ranking.

5.4. Computational complexity metrics

Most of the present day applications of BFG need to operate with limited amount of memory and computations. This metric aims to quantify the

1. Memory: number of variables required to define the OCV–SOC characterization
2. Computations: the computational complexity in finding the OCV for a specific SOC.

In Table 4, we list the number of parameters to be stored in memory as well as the computational requirements for calculating OCV for a given SOC in terms of the number of additions (add), number of floating point multiplications (mult) and the number of logarithmic computations (ln).

6. HIL data analysis

The *OCV–SOC characterization data* was gathered by hardware-in-the-loop experiments conducted on 9 different batteries at 16 different temperatures from −25 °C to +50 °C in steps of 5 °C using a Tenney thermal chamber and an Arbin BT-2000 cell test station. The battery manufacturers, battery types, number of batteries used in the experiment, and their rated capacities are summarized in Table 2.

Table 4
Memory and computational requirement of OCV–SOC models.

Model	Required memory	Computation: SOC → OCV
Shepherd model (2.1)	2	1 add + 1 mult
Unnewehr model (2.1)	2	1 add + 1 mult
Nernst model (2.1)	3	2 add + 2 mult + 2ln
Combined model (2.1)	5	4 add + 4 mult + 2ln
Combined+3 model (2.1)	8	7 add + 7 mult + 2ln
Polynomial model (2.1)	$L+1$	L add + L mult
Exponential model (2.1)	$L+1$	L add + L mult + Lexp
Chebyshev model (2.1)	L	1 add + 2 mult
Double exponential (2.2)	5	5 add + 3 mult + 2exp
Nonlinear exponential 2 (2.2)	6	1 add + 2 mult
Rational approximant (2.2)	2	1 add + 2 mult
Hybrid models (2.3)	Variable	Model dependent

For each cell, the data is collected in the following manner: First, the cell is rested at the test temperature at full charge. Then, the cell was discharged at C/30 rate until fully discharged to the minimum voltage (3 V) followed by a short rest period. Subsequently, the cell was charged at C/30 rate until fully charged (4.2 V). The low rates were used to minimize the cell dynamics. Some optional charge/discharge pulses (approximately C/3 rate) were used to determine (initialize) the cell resistances and time-constants. The OCV was computed by averaging the cell voltage as a function of SOC under discharge and charge. This eliminates the presence of hysteresis and ohmic resistance effects in the final OCV function.

Fig. 16 shows the typical OCV–SOC characterization data that is collected from one of the cells and the resulting OCV curve obtained.

Fig. 17 shows a sample OCV model obtained for a particular battery cell (cell 4 of Samsung EB575152) at 50 °C. The modeling error at a particular SOC is computed by subtracting modeled OCV from the average of measured voltages (during charging and discharging).

In Fig. 18, we give a comprehensive summary of OCV modeling showing the errors of different OCV modeling approaches, across different batteries and temperatures. First, the average value of the OCV modeling error of an each battery cell at each temperature is computed by averaging the OCV modeling error across all SOC values (i.e., by averaging the OCV modeling error shown in the bottom plot of Fig. 17). Then, in Fig. 18, the average error across all the battery cells listed in Table 2 is shown as a box plot[10] for each temperature. The Chebyshev model must be noticed for its smallest error across all temperatures and for its consistency across different batteries as indicated by the (compact) sizes of boxes and the lack of outliers across all temperatures.

The results of the model evaluation metrics and error metrics have been combined and presented in Table 5. The Chebyshev model performs the best among all the models based on the metrics presented in the paper.

7. Conclusions

This paper presented several approaches and analysis related to the open circuit voltage characterization of Li-ion batteries with a special emphasis on mobile and wearable electronic device

[10] Using box plot function in Statistics Toolbox of Matlab. On each box, the central mark is the median, the edges of the box are the 25th and 75th percentiles, the whiskers extend to the most extreme data points not considered outliers, and outliers are plotted individually.

Table 5
Model selection metrics rankings.

OCV Model	Rankings									
	AIC	AIC2	FPE	BIC	MDL	RMSE	R^2	BF	Max error	Borda
Chebyshev model	1	1	1	1	1	1	1	1	4	1
Rational approximant	2	2	2	2	2	2	2	2	5	2
Polynomial (4th order)	3	3	4	3	4	3	4	3	1	3
Hybrid model	5	5	3	4	3	4	3	4	2	4
Combined model	6	6	5	6	5	5	5	5	7	5
Exponential model	7	7	6	5	6	6	6	6	6	6
Nonlinear exponential model 2	8	8	7	7	7	7	7	8	9	7
Combined+3 model	4	4	12	11	12	7	11	7	3	8
Nernst model	9	10	8	8	8	9	8	9	10	9
Unnewehr universal model	11	11	9	10	9	10	9	10	11	10
Double exponential model	10	9	10	9	10	11	12	12	12	11
Shepherd model	12	12	11	12	11	12	10	11	8	12

applications. Memory and computational power becomes scarce (due to prioritization) for BFG in these applications, yet, the BFG capabilities such as prediction of time to shut down and remaining useful life are considered desirable features to have.

Offline characterization of open circuit voltage is crucial for BFG, especially in memory and computing power constrained electronic applications. We include several existing OCV modeling functions and many newly proposed OCV modeling approaches in a performance analysis in terms of OCV modeling accuracy, computational complexity and memory requirements.

It was discovered that significant savings in memory can be achieved by the proposed normalized OCV modeling, in which the SOC at each temperature is defined in terms of the temperature specific capacity. As a result, we found that, the OCV–SOC characterization remains practically the same regardless of the temperature or age of the battery. This finding is crucial for online battery capacity estimation, i.e., the normalized OCV parameters will serve as a means for accurate, online battery capacity estimation, such as the one presented in Ref. [2].

Apart from the benefits in mobile applications, the normalized OCV modeling approach reported in this paper has impact on other applications such as in electric vehicles and energy storage grid where accurate capacity estimation is critical.

Acknowledgments

We thank the anonymous reviewers for providing useful comments and suggestions that resulted in the improved quality of this paper. We would like to thank Mr. Curtis Guild and Prof. Steven Suib of the Department of Chemistry at the University of Connecticut for chemistry and composition characterization of the lithium-ion commercial cells. The work reported in this paper was partially supported by NSF grants ECCS-0931956 (NSF CPS), ECCS-1001445 (NSF GOALI), ARO grant W911NF-10-1-0369, and ONR grant N00014-10-1-0029. We thank NSF, ARO and ONR for their support of this work. Any opinions expressed in this paper are solely those of the authors and do not represent those of the sponsors. The authors would like to thank Prof. Gregory L. Plett of University of Colorado at Colorado Springs for the collection of the OCV–SOC characterization data.

References

[1] B. Balasingam, G.V. Avvari, B. Pattipati, K.R. Pattipati, Y. Bar-Shalom, J. Power Sources 219 (2014) 317–333.
[2] B. Balasingam, G.V. Avvari, B. Pattipati, K.R. Pattipati, Y. Bar-Shalom, J. Power Sources 269 (July 2014) 949–961.
[3] B. Balasingam, G.V. Avvari, B. Pattipati, K.R. Pattipati, Y. Bar-Shalom, J. Power Sources (2014) under review.
[4] N.A. Chaturvedi, R. Klein, J. Christensen, J. Ahmed, A. Kojic, IEEE Control Syst. Mag. 30 (3) (2010) 49–68.
[5] S.K. Rahimian, S. Rayman, R.E. White, J. Power Sources 196 (20) (2011) 8450–8462.
[6] M.A. Roscher, O. Bohlen, J. Vetter, Int. J. Electrochem. (2011) 1369–1384.
[7] M.A. Roscher, D.U. Sauer, J. Power Sources 196 (2011) 331–336.
[8] H. He, X. Zhang, R. Xiong, Y. Xu, H. Guo, Energy 39 (1) (2012) 310–318.
[9] R. Xiong, F. Sun, X. Gong, C. Gao, Appl. Energy 113 (2014) 1421–1433.
[10] Y.-H. Chiang, W.-Y. Sean, J.-C. Ke, J. Power Sources 196 (8) (2011) 3921–3932.
[11] G.V. Avvari, B. Balasingam, K. Pattipati, Y. Bar-Shalom, J. Power Sources (2014) under review.
[12] M. Petzl, M.A. Danzer, IEEE Trans. Energy Convers. 28 (3) (2013) 675–681.
[13] H. Dai, X. Wei, Z. Sun, J. Wang, W. Gu, Appl. Energy 95 (2012) 227–237.
[14] Y. Xing, W. He, M. Pecht, K.L. Tsui, Appl. Energy 113 (2014) 106–115.
[15] I. ThermoAnalytics, Battery Modeling @ONLINE, September 2012. URL: http://www.thermoanalytics.com/docs/batteries.html.
[16] S. Moore, M. Ehsani, SAE Tech. Pap. 105 (6) (1996) 421–424, 960448.
[17] L.E. Unnewehr, S.A. Nasar, Electric Vehicle Technology, John Wiley & Sons, 1982.
[18] K.P. Ta, J. Newman, J. Electrochem. Soc. 146 (8) (1999) 2769–2779.
[19] M. Verbrugge, E. Tate, J. Power Sources 126 (2004) 236–249.
[20] G.L. Plett, J. Power Sources 134 (2) (2004) 262–276.
[21] A. Szumanowski, Y. Chang, IEEE Trans. Veh. Technol. 57 (2008) 1425–1432.
[22] W.H. Press, B.P. Flannery, S.A. Teutolsky, W.T. Vetterling, Numerical Recipes: the Art of Scientific Computing, Cambridge University Press, 1990.
[23] M. Abramowitz, I.A. Stegun, Handbook of Mathematical Functions, Dover Publications, Inc., 1964.
[24] K.S. Khattri, Teach. Math. 12 (1) (2009) 7–14.
[25] Y. Hu, S. Yurkovich, Y. Guezennec, B.J. Yurkovich, J. Power Sources 196 (2011) 449–457.
[27] M. Chen, G. Rincón-Mora, IEEE Trans. Energy Convers. 21 (2006) 504–511.
[28] S.V. Huffel, in: COMPSTAT Proceedings in Computational Statistics, Physika-Verlag, Heidelberg, 2004, pp. 539–555.
[29] I. Markovsky, S.V. Huffel, Int. J. Signal Process. 87 (2007) 2283–2302.
[30] I. Markovsky, D.M. Sima, S.V. Huffel, Wiley Interdiscip. Rev. Comput. Stat. 2 (2) (2010) 212–217.
[31] Wikipedia, Nameplate Capacity @ONLINE, July 2013. URL: http://en.wikipedia.org/wiki/Nameplate_capacity.
[32] K.P. Burnham, D.R. Anderson, Model Selection and Inference, Springer-Verlag, 1998.
[33] J.-C. de Borda, Memoire sur les elections au scrutin, Histoire del'Academie Royale des Sciences.